Effect of Environmental Factors on the Mechanical Properties of Grafted Casein Films: Influence of Temperature and Extension Rate

N. SOMANATHAN

Biophysics Laboratory, Central Leather Research Institute, Adyar, Madras 600 020, India

SYNOPSIS

Casein was grafted with acrylonitrile (AN) and with a binary mixture of acrylonitrile and *n*-butyl methacrylate (*n*-BMA). Stress–strain characteristics of these films were analyzed as a function of temperature and rate of extension. The results shows that both the systems are sensitive to temperature. Due to the incorporation of *n*-BMA, the material becomes flexible since the T_g of the multiphasic polymer was reduced and therefore shows the changes even at lower temperatures when compared to casein grafted with AN. The fracture morphologies of the binary mixture-grafted casein films show that the effect produced by temperature and rate of extension are inversely related. © 1994 John Wiley & Sons, Inc.

INTRODUCTION

Casein, a glycoprotein, has wide-application potential in paper, textile, and leather industries. For leather, casein film is used as a finish. Though this material has very good properties for a finish, it also has two major drawbacks, viz., brittleness and hydrophilicity. Grafting of casein, with suitable monomers, is done to improve brittleness and hydrophilicity problems.

Grafting of natural polymers like gelatin, silk, wool, and collagen has been a topic of great interest.[1–10] Like other biopolymers, casein is also grafted with monomers to modify the properties. Acrylic[11–17] and methacrylic[18–20] monomers were used for grafting casein. The properties of the chinon fibers, which are made from acrylonitrile-grafted casein, has been reviewed by Morinaoto Saichi.[21] Acrylonitrile has been grafted onto casein and the amino acid analysis and the mechanism of polymerization has been reported by Kulasekaran et al.[22] and Jinyu and Ning.[23]

Acrylonitrile (AN) grafting of casein is advantageous compared to other monomers. Casein grafted with AN forms into a glazable film[17] when compared to casein grafted with other acrylic monomers.[24] In spite of extensive studies on the chemical aspects of AN-grafted casein films, little attention has been paid to the analysis of the mechanical behavior under processing and end-use conditions. The physical properties[25] of polymers are governed by several variables such as temperature, the rate of straining, plasticization, molecular weight, dimensions of the specimen, and previous history of loading.

The stress–strain properties of polymers are sensitive to temperature and strain rate. In general, the modulus, yield strength, and tensile strength decrease with the increase of temperature. When the strain rate increases, the tensile strength and modulus increase, whereas the breaking strain decreases. Increase in the rate of deformation has an effect that is similar to that of a decrease in temperature.[25,26] Since temperature and strain rate affect the tensile properties, much work[27–30] has been carried out on these lines, a knowledge of which forms the basis for most application purposes. The strain-rate effect on the mechanical properties of polystyrene, polycarbonate, and polyethylene has been reported in detail.[31–33] Investigations on the interrelationship of the rate of crack propagation and strain rate have also been reported.[34,35] Casein, when used for leather finishing, is subjected to friction glazing and this

Journal of Applied Polymer Science, Vol. 52, 1069–1079 (1994)
 CCC 0021-8995/94/081069-11

process generates heat and ultimately raises the surface temperature. In the finished product, under normal usage, the casein-finish films are subjected to different strain levels. Hence, it is important to study the influence of temperature and strain rate on the stress–strain characteristics of grafted casein film. In this present investigation, the influence of these two factors on the stress–strain behavior of casein grafted with AN and casein grafted with binary mixture of AN and *n*-butyl methacrylate (*n*-BMA) are reported.

EXPERIMENTAL

Preparation of 10% Casein Solution

Casein (2.5 g) was soaked overnight in water (25 mL). It was then gradually treated with a solution of triethanolamine (0.5 g) in water (10 mL). After the casein was dissolved completely, the solution was cooled. The pH of this solution was 7.75. This 10% solution was used in the preparation of graft copolymers.

Preparation of Graft Copolymers

Grafting was done with AN in the first set of experiments and with the binary mixture of AN and *n*-BMA in the second experiment, following the procedure discussed in our earlier publication.[36] A three-necked R.B. flask fitted with a mechanical stirrer, a water condenser, a thermometer, a nitrogen inlet, and two dropping funnels was placed in a water bath maintained at a temperature of 60°C. Nitrogen was bubbled through the solution throughout the reaction. The monomer was placed in one of the dropping funnels. The concentration of the monomer in the case of AN was 2 mol L^{-1}. In the case of the binary mixture, first the binary mixture was prepared by mixing 0.9 mol of AN and 0.1 mol of *n*-BMA, and 1.2 mol L^{-1} of this mixture was used. The initiator, potassium persulfate, was dissolved in water (9.7×10^{-3} mol L^{-1}) and taken in the second dropping funnel. The monomer concentration, temperature of the reaction, and initiator concentration were fixed on the basis of our earlier studies,[37,38] at which the maximum percent grafting and grafting efficiency were obtained. The temperature and time of reaction were 60°C and 3 h, respectively. The reaction mixture obtained from the grafting reaction was made into films without separating the homopolymer, in order to simulate the end-use condition.

Film Formation

Films were cast on the Hg surface at 65% RH. The film was removed from the Hg bed, dried in vacuum, and conditioned for 7 days in a desiccator. Dumbbell-shaped specimens were cut as per ASTM standards.[39]

Mechanical Testing

The stress–strain characteristics of grafted casein films were studied using an Instron universal tensile tester (Model 1112). For studying the effect of temperature, a thermostatic test chamber surrounding the specimen and the grips was used. The detailed testing procedure has been discussed in an earlier publication.[40] For temperature studies, samples were tested at an extension rate of 0.5 cm/min.

To study the effect of strain rate, testing was done at 25°C and 65% RH. The rate of extension was varied from 0.05 to 20 cm/min.

Morphologies of the samples fractured at different temperatures and strain rates were studied using a Stereoscan S 150 scanning electron microscope.

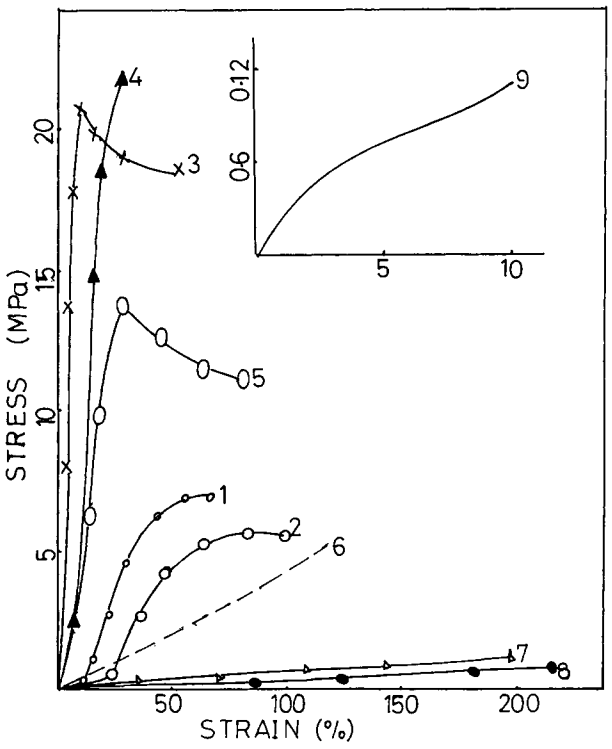

Figure 1 Stress–strain curves of Ca-*g*-AN at different temperatures (°C): (1) 10; (2) 20; (3) 28; (4) 40; (5) 60; (6) 80; (7) 100; (8) 120; (9) 140.

Table I Tensile Properties of Ca-*g*-AN at Different Temperatures

Temperature (°C)	Stress at Break (MPa)	Strain at Break (%)	Energy to Break (MJ/m^3)
10	7.23	67.1	2.88
20	5.72	98.8	3.50
28	18.93	51.4	9.30
40	22.03	28.2	3.00
60	12.35	79.2	8.40
80	5.15	114.0	2.80
100	2.03	192.0	1.23
120	0.79	215.3	0.60
140	0.11	11.1	0.06

RESULTS AND DISCUSSION

Effect of Temperature

Stress–strain characteristics of the AN-grafted casein films tested at different temperatures are presented in Figure 1. The stress at break increases to a maximum value at 40°C and then decreases, whereas the strain at break shows a reverse trend. At lower temperatures, the stress at break is low and the stress–strain curves show only a pseudo yield point. At 28°C, there is a pronounced yield point, and after the formation of the neck, the sample breaks, before the neck could restabilize. At 40°C, the sample breaks even before the formation of the neck. With the increase in temperature from 40 to 60°C, the strain at break increases from 28 to 79%. Thereafter, the strain continuously increases and the stress decreases with the increase in temperature (Table I).

The energy-to-break value increases to a maximum value and then decreases with a further increase of temperature. The energy value shows a sudden decrease at 40°C, which suggests that the fracture behavior is different, when compared to the behavior at 28°C.

Stress–strain curves of casein grafted with the binary mixture[40] are presented in Figure 2. At 28°C, there is a pseudo yield point, and after that point, the strain increases rapidly with a marginal increase

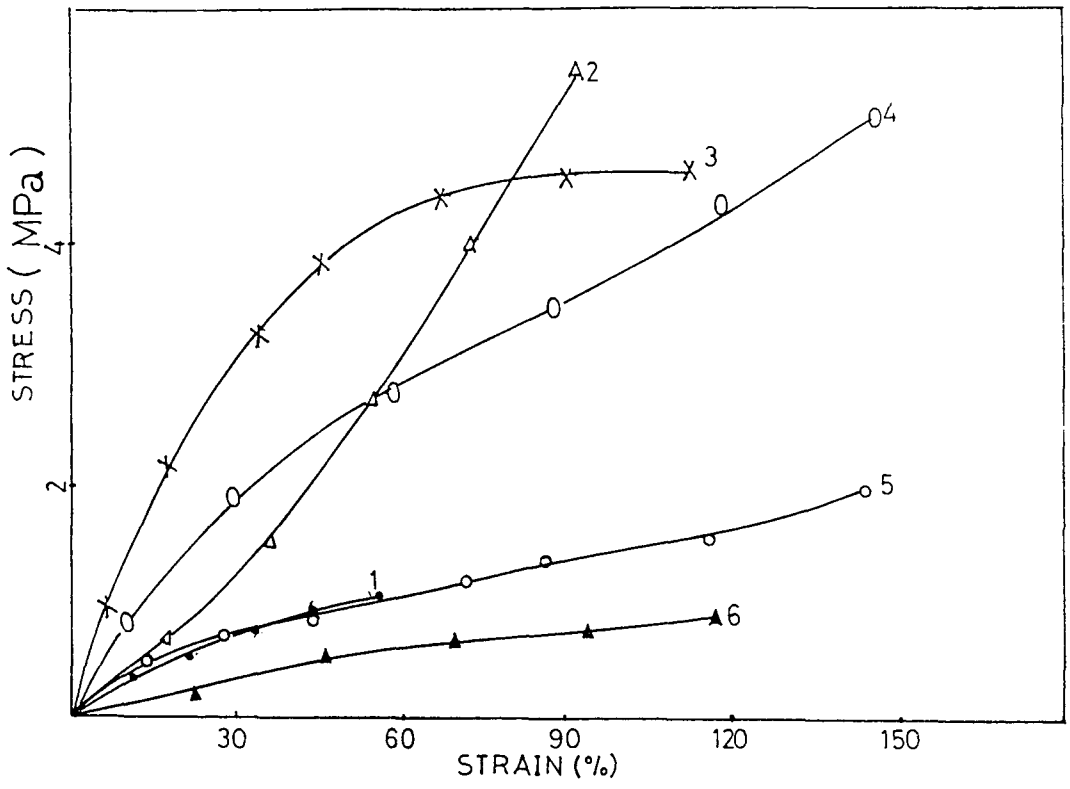

Figure 2 Stress–strain curves of Ca-*g*-AN-*co*-*n*-BMA at different temperatures (°C). (1) 10; (2) 20; (3) 28; (4) 50; (5) 70; (6) 100.

Table II Energy-to-break Values Calculated from Stress–Strain Graphs of Ca-*g*-AN-*co*-*n*/BMA

Temperature (°C)	Energy to Break (MJ/m^3)
10	0.36
20	1.88
28	3.84
50	4.23
70	1.55
100	0.53

in stress. At other temperatures, there is uniform extension. The low values of tensile strength at 10°C can be attributed to the presence of polar groups in the polymer.[41] The stress increases with increase in temperature, reaches a maximum at 28°C, and then decreases. A similar trend is also followed by strain at break and the maximum strain value is obtained at 50°C.

The energy-to-break values calculated from stress–strain curves (Table II) shows an increase to a maximum and then a decrease when the temperature is increased. The maximum value for energy to break is obtained at 50°C.

When the stress–strain behavior of Ca-*g*-AN (Fig. 1) is compared to Ca-*g*-AN-*co*-*n*-BMA (Fig. 2), in general, there is a marked shift from brittle to ductile behavior. At lower temperature, there is a twofold increase in strain at break, in the case of binary mixture-grafted casein, even though there is a significant decrease in stress at break. This can be attributed to the presence of *n*-BMA molecules, since the humidity level absorbed by both the systems at 65% RH is the same.[37] The stress and energy to break were considerably decreased and the strain at break was increased due to the incorporation of *n*-BMA.

To obtain greater insight into the effect of temperature, morphological studies were undertaken on samples fractured at different temperatures. In Figures 3 and 4, the surface morphologies of Ca-*g*-AN and Ca-*g*-AN-*co*-*n*-BMA are presented. At 28°C [Fig. 3(a)], the surface shows a structure similar to craze lines near the fracture edge. Apart from craze lines, characteristic localized shear yield failure lines are also seen at 40°C [Fig. 3(b)]. Due to its mutual resultant effect, the material failure has probably been locally initiated even before yield point (Fig. 1). The surface structure of the film tested at 100°C is shown in Figure 3(c). The surface morphology shows that the material has flown toward the direction of stress application, leading to microcrack formation in the material, as also indicated by the stress–strain curves.

Figure 3(c) suggests that there could be more than one microphase[42] in the system and the failure possibly occurs near the interface of the microphases present in the system. The morphology of the fractured edge of Ca-*g*-AN at 28 and 100°C is presented in Figure 3(d) and (e), respectively. The morphology at 28°C [Fig. 3(c)] shows a failure characteristic of brittle failure. Stress–strain curves (Fig. 1) also show that the stress and the energy taken by the system is very high. Figure 3(d) shows that at 100°C the material has flown, as is also clearly indicated by an uniform extension in stress–strain behavior (Fig. 1).

The surface structures of Ca-*g*-AN-*co*-*n*-BMA samples tested at 28, 50, and 100°C are presented in Figure 4(a), (b), and (c), respectively. The morphology of the fracture edge tested at 28 and 100°C are given in Figure 4(d) and 4(e), respectively. The fractured edge (cross section) morphology at 28°C shows hill- and valleylike structures, suggesting that the failure is of ductile type. Similar morphology is seen on the samples tested at 20 and 50°C. Figure 4(e) shows that the fractured ends join together to form an agglomer. The agglomer orients in a direction perpendicular to the direction of stress application.

The morphology of the samples tested at different temperatures suggest that after 50°C a possible transition takes place in the sample, and because of that, the material flows. This is also evident from stress–strain curves (Fig. 3). The orientation of the lamellar structure is also seen on the surface of the samples tested at 100°C [Fig. 4(e)], whereas the surface morphology is totally different at 50°C. The morphology indicates that the response of different components of the system to temperature changes are different and, hence, the multiphasic nature of this Ca-*g*-AN-*co*-*n*-BMA is noted in Figure 4(b).

Comparison of Figures 3(d) and 4(d) clearly indicates the influence of *n*-BMA on the fracture morphology. Figure 3(d) shows the characteristic brittle fracture surface, whereas the fracture changes to ductile fracture [Fig. 4(d)] due to the incorporation of *n*-BMA. Even at 100°C, the morphology shows a characteristic change [Figs. 3(e) and 4(e)]. The meltinglike and flowing behavior is very much pronounced due to the incorporation of *n*-BMA. This may possibly be due to the reduction in tran-

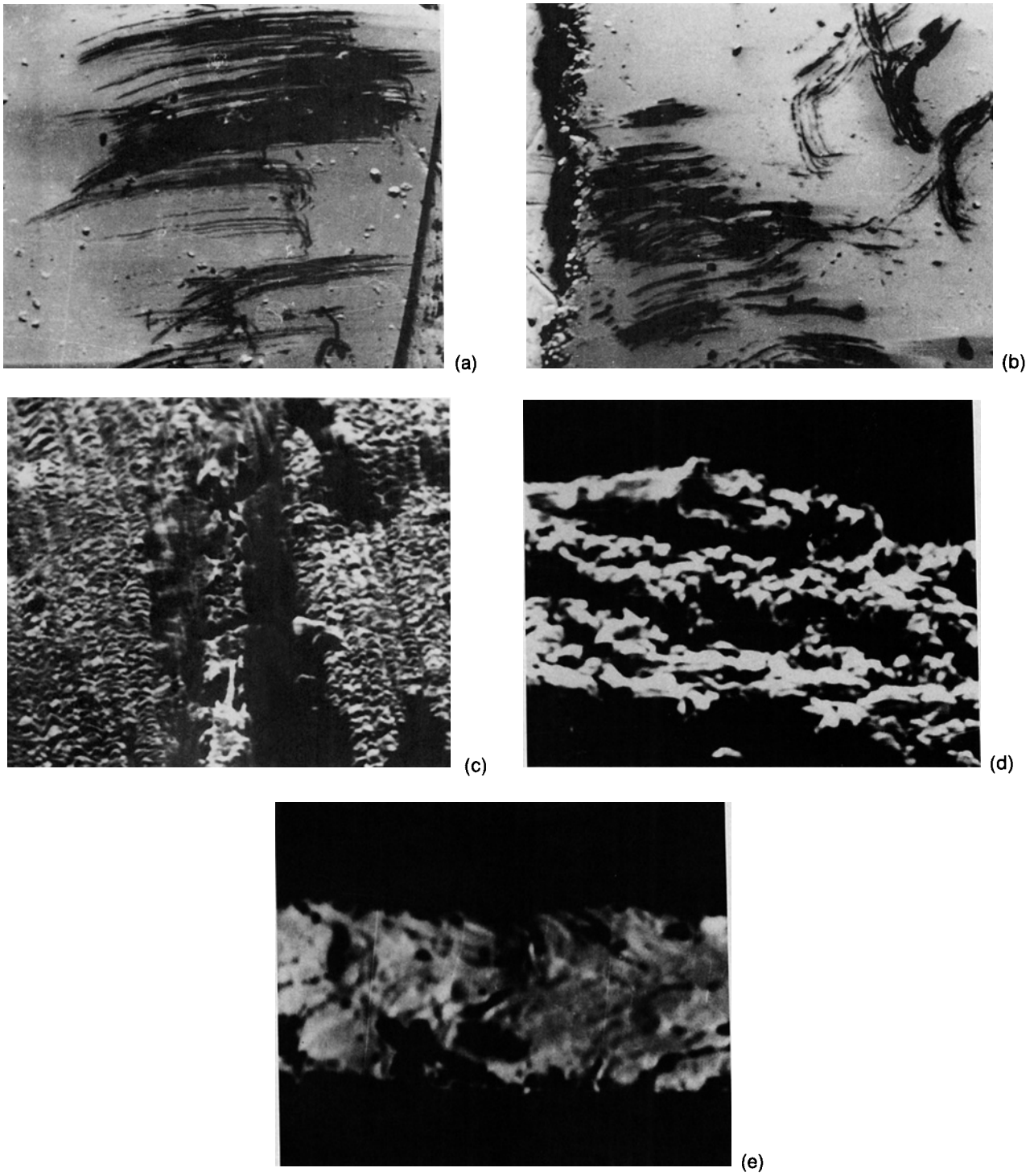

Figure 3 (a–c) SE micrographs showing the fractured surface morphologies of Ca-*g*-AN at different temperatures (°C): (a) 28 (60×); (b) 40 (60×); (c) 100 (350×). (d–e) SE micrographs showing the fractured-edge morphologies of Ca-*g*-AN at different temperatures (°C): (d) 28 (450×); (e) 100 (450×).

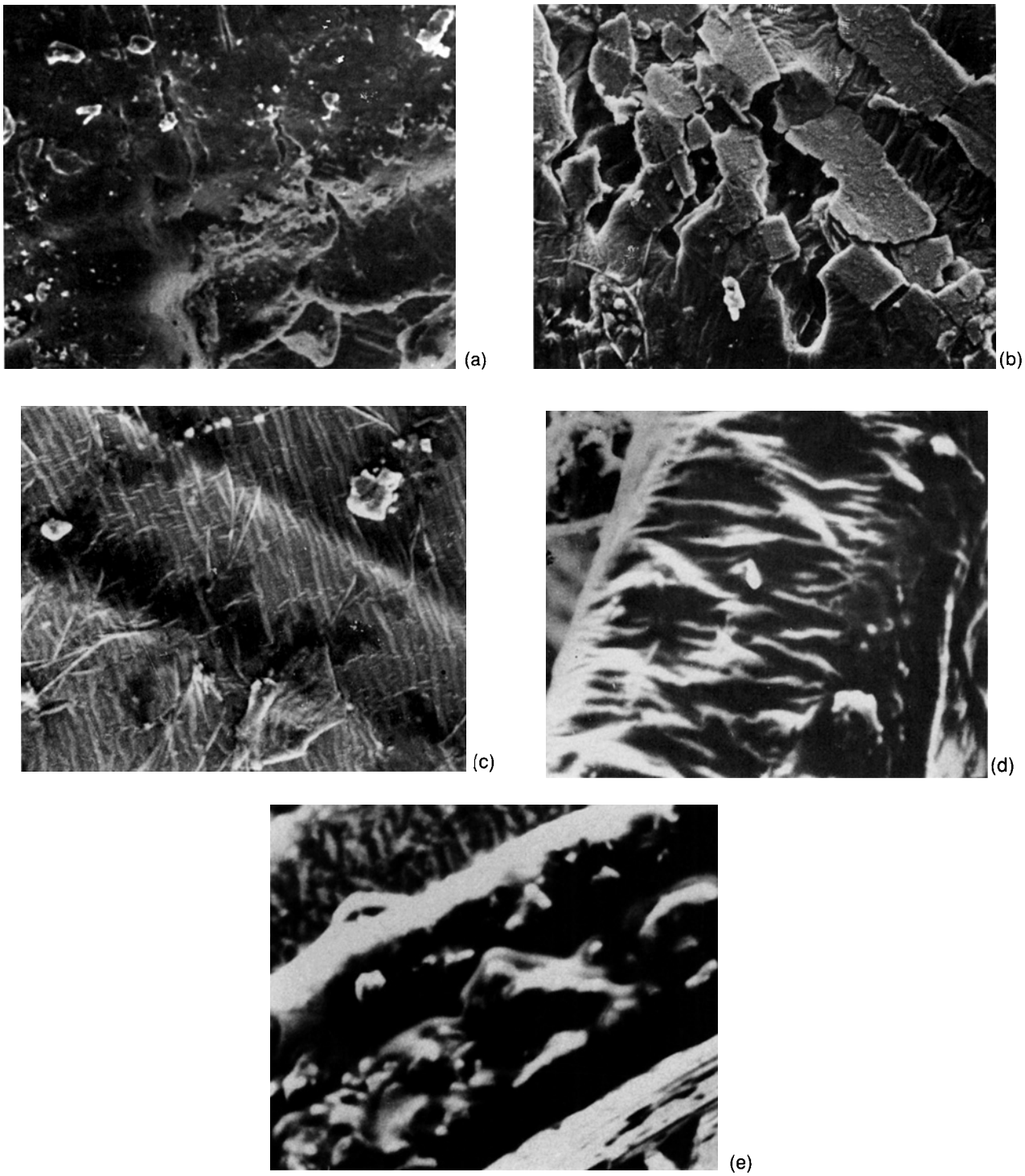

Figure 4 (a–c) SE micrographs showing the fractured surface of Ca-*g*-AN-*co*-*n*-BMA at different temperatures (°C): (a) 28 (600×); (b) 50 (600×); (c) 100 (600×). (d–e) SE micrographs showing the fractured edge of Ca-*g*-AN-*co*-*n*-BMA at different temperatures (°C): (d) 28 (600×); (e) 100 (600×).

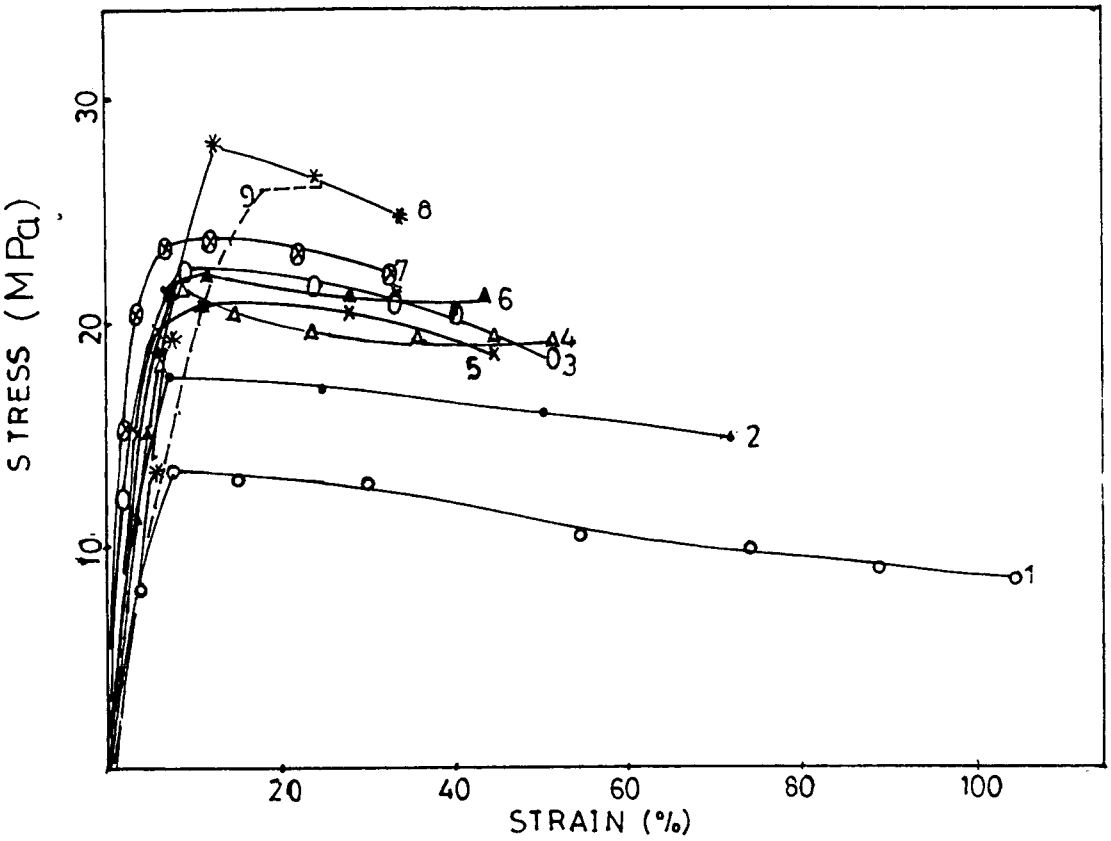

Figure 5 Stress–strain characteristics of Ca-*g*-AN tested at different extension rates (cm/min): (1) 0.05; (2) 0.125; (3) 0.25; (4) 0.5; (5) 1.0; (6) 2.0; (7) 5.0; (8) 10.0; (9) 20.

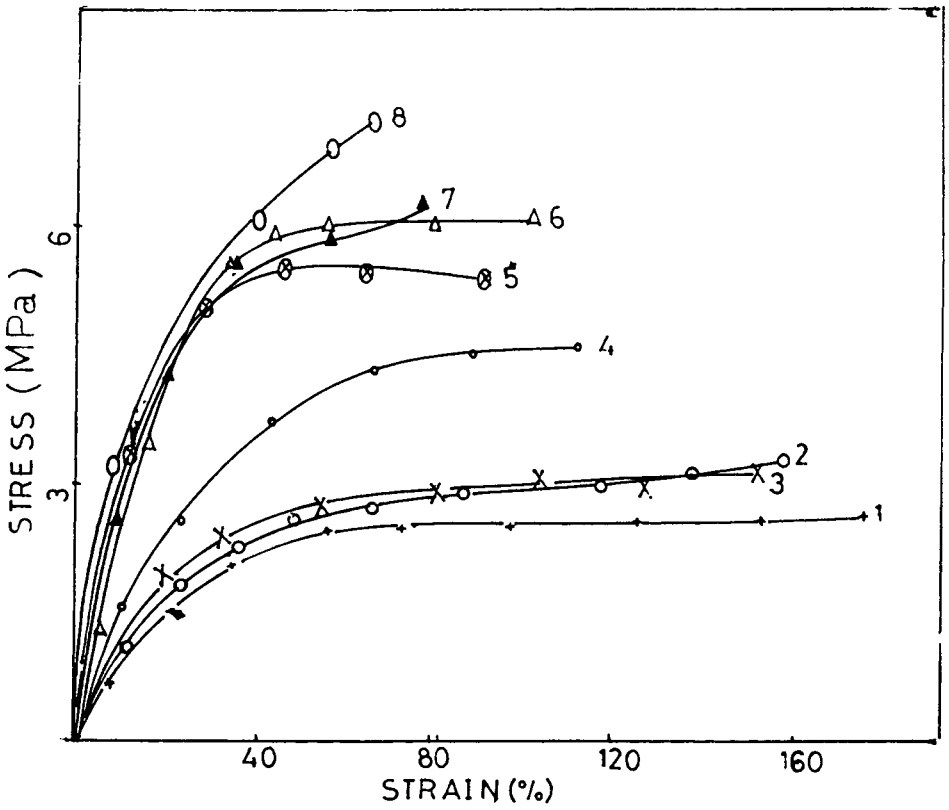

Figure 6 Stress–strain curves of Ca-*g*-AN-*co*-*n*-BMA, tested at different extension rates (cm/min): (1) 0.05; (2) 0.125; (3) 0.25; (4) 0.5; (5) 1.0; (6) 5.0; (7) 10.0; (8) 20.0.

Table III Tensile Properties of Ca-*g*-AN at Different Strain Rates

Strain Rate (per min)	Stress at Break (MPa)	Strain at Break (%)	Energy to Break (MJ/m^3)
0.05	9.25	104.0	11.1
0.125	14.70	71.9	11.5
0.25	18.18	52.2	10.1
0.5	18.91	51.4	9.3
1.0	18.42	44.9	8.6
2.0	20.58	42.8	8.4
5.0	21.95	32.5	7.0
10.0	24.30	34.2	7.4
20.0	25.09	24.5	4.1

sition temperature on incorporation of low T_g polymer.

To understand the effect produced by the extension rate, the samples were analyzed at different strain rates. Stress–strain curves of Ca-*g*-AN and Ca-*g*-AN-*co*-*n*-BMA, tested at different extension rates, are presented in Figures 5 and 6, respectively. In the case of Ca-*g*-AN, there is a yield point at all extension rates. The strain at break decreases with the extension rate and the stress–strain curves shift toward the stress axis. In the case of extension at break, a reversal in trend is seen (Table III). The energy-to-break values continue to decrease with increase of the extension rate. In general, the rate of change of strain is very high when compared to stress. This suggests that the strain is very much influenced by the extension rate in the case of Ca-*g*-AN.

The stress–strain behavior in the case of binary mixture-grafted casein also shows a shift toward the stress axis with increasing extension rate. However, even at a higher extension rate, the material does not exhibit brittle behavior and shows a pseudo yield point, in contrast to the Ca-*g*-AN system. The energy-to-break (Table IV) values initially increase, and after reaching a maximum, tend to decrease with increase of the extension rate.

Comparison of Figures 5 and 6 suggests that due to the incorporation of soft polymer (*n*-BMA) the energy absorbed by the system is considerably decreased. At all strain rates, the stress at break is considerably reduced. At lower strain rates, there is a characteristic change in strain values in the case of Ca-*g*-AN, whereas in the case of Ca-*g*-AN-*co*-*n*-BMA, it is not much affected.

Morphological studies were done with samples fractured at different extension rates and are presented in Figures 7 and 8 for Ca-*g*-AN and Ca-*g*-AN-*co*-*n*-BMA, respectively. Figure 7(a) and (b) show the surface morphology of the samples tested at a 0.05 cm/min extension rate. The optical micrographs show that there are more than one microphase and that they react to stress in different ways. Figure 7(b) shows that the cracks possibly propagate from the rigid microphase to the other phase. At lower extension rates, after yielding, there is necking followed by cold drawing (Fig. 5), whereas at higher extension rates, there is no restabilization of the neck. These features are reflected on the fracture edge morphology [Fig. 7(d)]. At lower extension rates, the fracture takes place very slowly in the neck region and the material orients toward the fractured tip and there is time for the sample to relax and reorient. At higher extension rates, there is neither time for restabilization of the neck nor time to relax and, therefore, the failure occurs abruptly. Figure 7(d) shows that the material after failure aggregates into an agglomerlike structure. This may be due to the fact that at higher strain rates conversion of inelastic work into heat could have occurred, resulting in an adiabatic temperature increase.[43–45] This heat would have caused a localized temperature increase and melted the material, which, on cooling, would have formed into an agglomer.

The fracture surface and fracture edge morphologies of Ca-*g*-AN-*co*-*n*-BMA at 0.05 and 20 cm/min extension rates are presented in Figure 8. At a 0.05 cm/min extension rate, the sample has a lamellar structure, showing the separation of the two phases. Figure 8(b) shows a rough morphology with the crack propagating in the direction of stress and also shows the heterogeneity of the material.

The fractured edge of samples tested at 20/min strain rate shows agglomerated structures similar to the one seen with Ca-*g*-AN [Fig. 7(d)]. Comparison

Table IV Energy Values Calculated from Stress–Strain Graphs of Ca-*g*-AN-*co*-*n*/BMA Tested at Different Strain Rates

Strain Rate (per min)	Energy to Break (MJ/m^3)
0.05	3.87
0.125	3.81
0.25	3.92
0.5	3.84
1.0	5.05
5.0	4.21
10.0	3.58
20.0	3.48

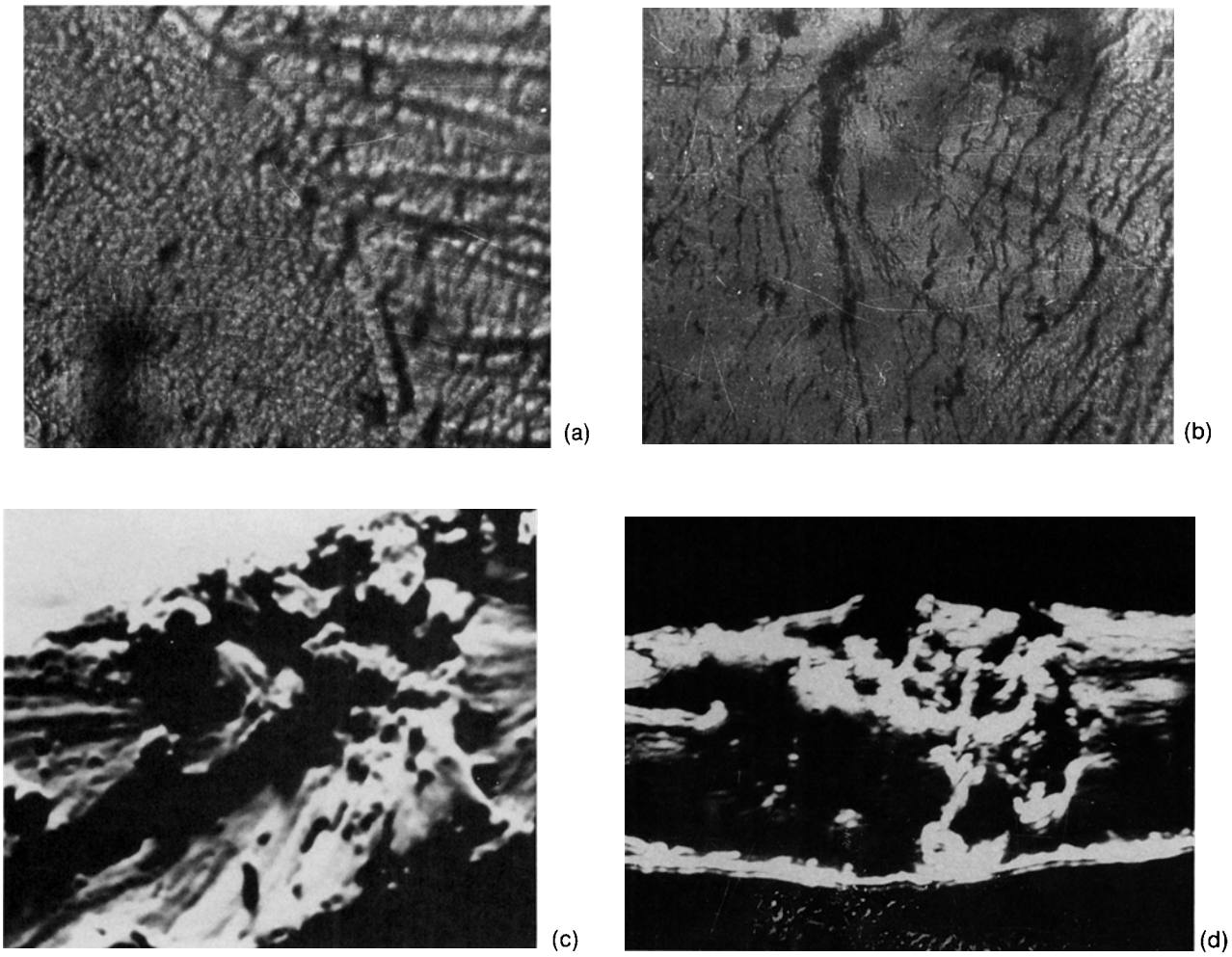

Figure 7 (a,b) Optical micrographs showing the fracture surface morphology of Ca-*g*-AN, tested at 0.05 cm/min extension rate (20×). (c,d) SE micrographs showing the fractured-edge morphologies of Ca-*g*-AN at various extension rates (cm/min): (c) 0.05 (450×); (d) 20.0 (450×).

of Figures 7(d) and 8(d) suggests that the agglomerated structures (due to thermal softening) are more numerous in Ca-*g*-AN-*co*-*n*-BMA when compared to Ca-*g*-AN [Fig. 7(d)]. This may be due to the incorporation of *n*-BMA, which reduces the T_g of the system. The fractured-edge morphology of the samples fractured at lower extension rates (0.5 cm/min) shows the predominance of silver streaks. It has been shown[46] that silver streaks form at places where there is considerable cold elongation and consolidation under prolonged stresses. With the increase of speed of deformation, the sample fails more quickly than does the formation of silver streaks, and at a still higher speed of deformation, they disappear altogether.

Comparison of the morphologies of the Ca-*g*-AN-*co*-*n*-BMA samples fractured at higher temperature [Fig. 4(c)] to the morphology of the samples fractured at lower strain rates [Fig. 8(a)] clearly reflects the inverse relationship between the effects of temperature and strain rate.

These studies reveal that the stress–strain behavior of casein, grafted with acrylonitrile, is very much influenced by temperature and strain rate. Due to the incorporation of *n*-BMA, the material becomes flexible. The mechanical properties of casein grafted with a binary mixture of monomers clearly show the inverse relationship between temperature and strain-rate effect in the experimental working range.

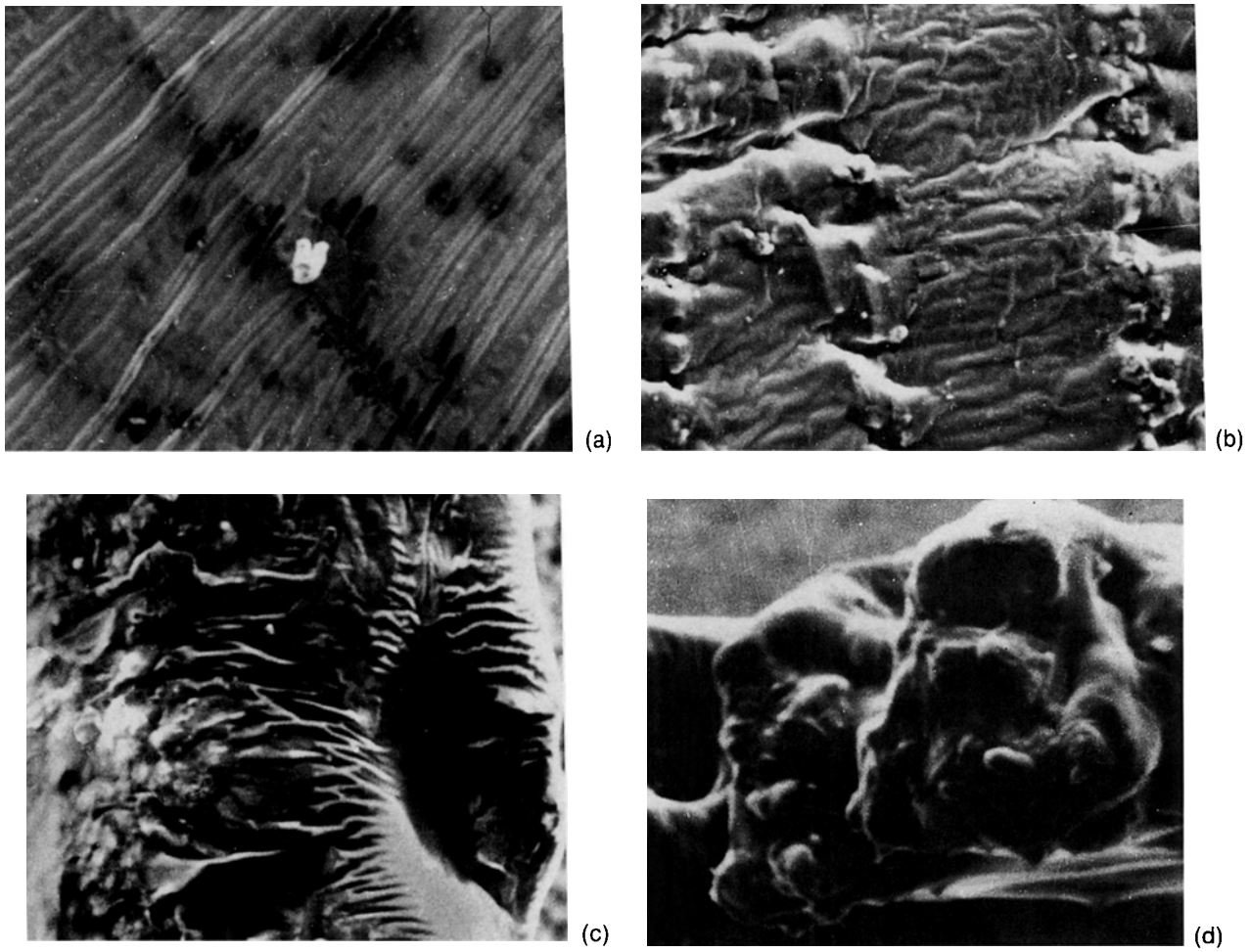

Figure 8 (a,b) SE micrographs showing the fractured-surface morphologies of Ca-*g*-AN-co-*n*-BMA at different extension rates: (a) 0.05 (650×); (b) 20.0 (650×). (c,d) SE micrographs showing the fractured edge morphology of Ca-*g*-AN-*co*-*n*-BMA at various extension rates: (c) 0.05 (650×); (d) 20.0 (650×).

The author thanks Dr. M. D. Naresh for his help during the preparation of this manuscript.

REFERENCES

1. M. D. K. Kumaraswamy, K. Panduranga Rao, and K. T. Joseph, *Eur. Polym. J.*, **16,** 353 (1980).
2. T. Kuwajima, H. Yoshida, and K. Hayashi, *J. Appl. Polym. Sci.*, **20,** 967 (1976).
3. A. George, G. Radhakrishnan, and K. T. Joseph, *J. Appl. Polym. Sci.*, **29,** 703 (1984).
4. J. Stejski, D. Strakova, and P. Kratochvil, *J. Appl. Polym. Sci.*, **36,** 215 (1988).
5. B. N. Mishra, A. S. Singha, and R. K. Sharma, *J. Appl. Polym. Sci.*, **27,** 1321 (1982).
6. J. S. Shulka, S. C. Tiwari, and G. K. Sharma, *J. Appl. Polym. Sci.*, **24,** 191 (1987).
7. J. S. Shukla and S. C. Tiwari, *J. Appl. Polym. Sci.*, **38,** 291 (1989).
8. L. I. Butina, M. V. Shisukina, S. F. Sadova, and M. V. Karchagin, *Vysokermel. Soedin Ser. A,* **17,** 150 (1975).
9. N. Y. Abou-Zeid, A. Kigazy, and A. Hebeish, *Angew. Macromol. Chem.*, **121,** 69 (1984).
10. A. Bazuaye, F. E. Okieimen, and O. B. Said, *J. Polym. Sci. Polym. Lett. Ed.*, **27,** 433 (1989).
11. D. Mohan, G. Radhakrishnan, and S. Rajadurai, *J. Macromol. Sci. Chem.*, **A20,** 201 (1983).
12. D. Mohan, G. Radhakrishnan, and T. Nagabhushanam, *J. Appl. Polym. Sci.*, **25,** 1799 (1980).
13. D. Mohan, G. Radhakrishnan, S. Rajadurai, T. Nagabhushnam, and K. T. Joseph, *J. Appl. Polym. Sci.*, **29,** 329 (1984).

14. D. Mohan, G. Radhakrishnan, S. Rajadurai, K. Venkata Rao, and G. G. Cameron, *J. Polym. Sci. Polym. Chem. Ed.*, **27,** 2123 (1989).
15. K. Stundriarski, W. Wyboz, and M. Swiekatowski, *Przegl Skorzany,* **38,** 235 (1983).
16. D. Mohan, G. Radhakrishnan, and S. Rajadurai, *Leather Sci.,* **33,** 242 (1986).
17. S. Valliappan, S. Rajadurai, and M. Santhappa, *Leather Sci.,* **22,** 1 (1975).
18. D. Mohan, G. Radhakrishnan, and S. Rajadurai, *J. Macromol. Sci. Chem.,* **A22,** 75 (1985).
19. K. Stundriarski, Z. Wilmanski, and P. Siwiek, *Przegl Skorzany,* **38,** 31 (1983); *Chemical Abstr.,* **100,** 23299b (1984).
20. S. Valliappan, S. Kulasekaran, S. Rajadurai, K. T. Joseph, and M. Santappa, *Leather Sci.,* **23,** 57 (1976).
21. M. Saichi, *Ind. Eng. Chem.,* **62,** 23 (1970).
22. A. Kulasekaran, Y. Lakshiminarayana, S. Rajadurai, K. T. Joseph, and M. Santappa, *Leather Sci.,* **23,** 383 (1976).
23. X. Jinyu and L. Ning, *Xibi Qiuggongye Xueyuan Xuebao,* **38,** 34 (1986); *Chem. Abstr.,* **110**(2) 8751f (1986).
24. D. Mohan, PhD Thesis, University of Madras, 1983.
25. I. M. Ward, *Mechanical Properties of Solid Polymer,* 2nd ed. Wiley-Interscience, New York, 1983.
26. N. M. Bikales, Ed., *Mechanical Properties of Polymer,* Encyclopedia reprints, Wiley-Interscience, New York, 1971.
27. V. Arumugam and R. Sanjeevi, *J. Mater. Sci.,* **22,** 2691 (1987).
28. F. J. Morgan, *J. Polym. Sci.,* **11,** 1271 (1973).
29. J. K. Kocsis and K. Friederich, *Polymer,* **27,** 1753 (1986).
30. M. Yokouchi, J. Mori, and Y. Kobayashi, *J. Appl. Polym. Sci.,* **26,** 3435 (1981).
31. M. Yokouchi and Y. Kobayashi, *J. Appl. Polym. Sci.,* **26,** 431 (1981).
32. M. Yokouchi, H. Uchiyama, and Y. Kobayashi, *J. Appl. Polym. Sci.,* **25,** 1007 (1980).
33. D. B. Barry and O. Delatycki, *J. Appl. Polym. Sci.,* **38,** 339 (1989).
34. J. G. Williams and G. P. Marshall, *Proc. R. Soc. Lond. A,* **342,** 55 (1975).
35. G. P. Marshall, *Plast. Rubber Process. Appl.,* **2,** 169 (1982).
36. N. Somanathan, C. Rami Reddy, N. Radhakrishnan, and R. Sanjeevi, *Eur. Polym. J.,* **23,** 489 (1987).
37. N. Somanathan, PhD Thesis, University of Madras, 1991.
38. Y. Lakshminarayana, PhD Thesis, University of Patna, 1976.
39. *1980 Annual Book of ASTM Standards,* Part 35, D1708-79, American Society of Testing of Materials, Philadelphia, 1980.
40. N. Somanathan, V. Arumugam, and R. Sanjeevi, *Eur. Polym. J.,* **23,** 803 (1987).
41. T. S. Casewell and H. K. Nason, *Mod. Plast.,* **21,** 121 (1944).
42. S. L. Aggarwal, in *Processing Structure and Properties of Block Copolymers,* M. J. Folkes, Ed., Elsevier, Amsterdam, 1985, Chap. 1.
43. I. J. Gruntfest, *J. Polym. Sci.,* **18,** 449 (1955).
44. P. I. Vincent, *Polymer,* **1,** 7 (1960).
45. G. M. Barkenew and S. Yu. Zuyev, *Strength and Failure of Viselastic Materials,* Pergamon Press, New York, 1971.
46. L. E. Nielson, *Mechanical Properties of Polymers,* Reinhold, London, 1965.

Received July 7, 1993
Accepted November 20, 1993